Model Order Reduction for COMSOL - A Compact Model of a Wireless Power Transfer System

J. Pico, D. Hohlfeld, and T. Bechtold
Institute of Electronic Appliances and Circuits, Department of Computer Science and Electrical Engineering, University of Rostock,
Albert-Einstein Str. 2, 18059 Rostock, Germany, tamara.bechtold@uni-rostock.de

Abstract: This work presents the application of mathematical methods of model order reduction (MOR) for automatic generation of highly accurate, compact models for wireless power transfer (WPT) systems. A block two-sided Second Order Arnoldi (SOAR) algorithm was implemented to automatically compute a compact model, which is highly accurate, but demands several orders of magnitude smaller CPU time. Thus, it can be used for the co-simulation of the WPT setup with electrical circuitry
Keywords: Wireless power transfer, Model order reduction, Block two-sided second order Arnoldi, System-level simulation.

1. Introduction

Nowadays, a new technological trend towards Wireless Power Transfer is driven by modern applications, such as medical implants, mobile devices, electrical vehicles, drones, and home appliances, which all profit of cable-free energy supply [1].

Available charging systems for electrical vehicles (EVs), which use cables to connect the vehicle to the grid, feature many disadvantages, such as dirtiness, broken cables and necessity to establish an electrical connecting also during rainy weather. The latter also impose safety risks. To overcome those issues several WPT charging solutions have been implemented as reported in [2] and [3].

Inductive power transfer [4] is one of the most widely used methods for WPT. It employs the principle of magnetic induction as used in a transformer, by taking advantage of the resonant coupling effect among coils of two resonant inductor-capacitor circuits (see Figure 1).

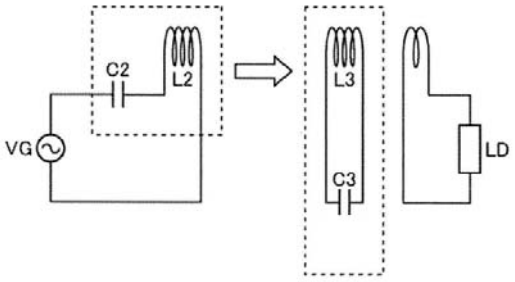

Figure 1. Resonant Inductive Coupling

In 2007, an initial report [5] demonstrated efficient WPT over distances up to eight times the radius of the coil. An efficiency of approximately 40% was reached over distances of 2 m (see Figure 2).

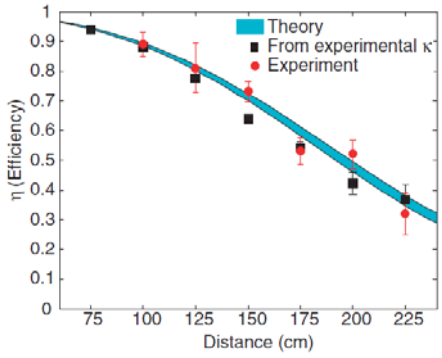

Figure 2. Comparison of experimental and theoretical efficiencies as functions of the WPT distance in [5].

Another experiment [6] considers aluminum plates located next to the resonant coils. The maximum efficiency larger than 94% was achieved over a distance of 60 cm, for a coil radius of 30 cm at a resonant frequency of 8.8 MHz (see Figure 3).

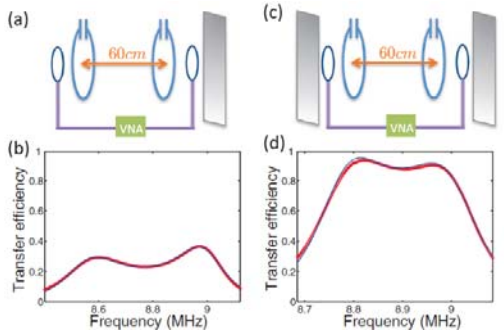

Figure 3. (a) WPT system in close proximity of an aluminum plate. (b) Transfer efficiency of WPT system with only a single metal plate (c) WPT system with two aluminum plates. (d) Transfer efficiency of WPT system with aluminum plates near both coils. Source: [6].

In 2014, a full recharging system was reported for EVs [7]. The system consisted of a pair of rectangular coils each attached to a ferrite layer, which magnetically shields the car (see Figure 4). Aluminum plates have been used as well, and it reaches a power efficiency of over 90%.

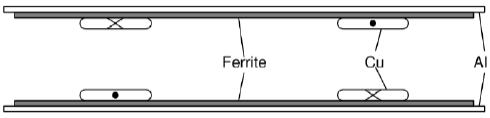

Figure 4. Magnetic designs for rectangular coils. Source: [7].

Our work aims at providing a system-level model of a WPT system for optimization of power transfer efficiency and tolerance analysis. In contrast to existing work [8] our contribution uses an accurate numerical model for the inductive component and enables time-efficient modeling by mathematical model order reduction

2. WPT Circuit Analysis

The WPT system consists of two inductively coupled coils. One inductor is connected to a power source, which drives a sinusoidal current. The voltage induced in the second inductor is supplied to a resistive load, which dissipates the transferred power. Matching capacitors are connected in series with the inductors to compensate for their impedance at the operating frequency In order to model and analyze such systems, traditionally equivalent circuits are used.

In Figure 5 a WPT an equivalent circuit is shown, with each coil being serially connected to a capacitor and a resistor. The latter represents the coil's inner resistance. Mutual inductance is marked with *M*.

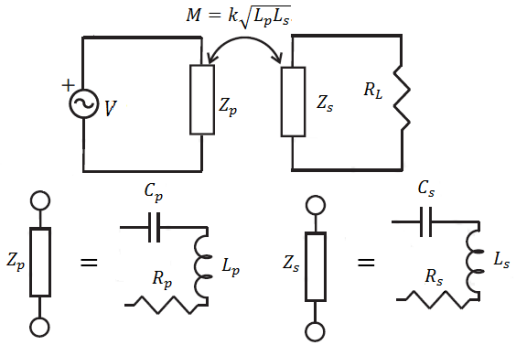

Figure 5. WPT equivalent circuit.

The resonance frequencies of both RLC-circuits, can be formulated as:

$$\omega_p = \frac{1}{\sqrt{L_p C_p}} \ , \omega_s = \frac{1}{\sqrt{L_s C_s}} \qquad (1)$$

A further equivalent circuit, with the mutual inductance represented as an inductor between primary and secondary resonator, is shown in Figure 6.

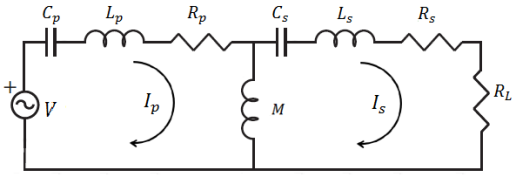

Figure 6. Equivalent circuit of coupled resonators.

The Kirchhoff's voltage law equations for primary and secondary circuits can be formulated as follows:

$$\begin{bmatrix} Z_p & j\omega M \\ j\omega M & Z_s + R_L \end{bmatrix} \begin{bmatrix} I_p \\ I_s \end{bmatrix} = \begin{bmatrix} V \\ 0 \end{bmatrix}$$

$$Z_p = R_p + j\omega L_p + 1/j\omega C_p \qquad (2)$$

$$Z_s = R_s + j\omega L_s + 1/j\omega C_s$$

From (2), the circuit input impedance can be defined as:

$$Z_{in} = \frac{V}{I_p} = \frac{Z_p(Z_s + R_L) + (\omega M)^2}{(Z_s + R_L)} \quad (3)$$

The reactance of the circuit becomes zero at resonance, and (3) yields a fourth degree polynomial with the following solutions (with $R_L = R_p = R_s = 0$):

$$\omega_{1,2,3,4} = \pm\sqrt{\frac{\omega_p^2 + \omega_s^2 \pm \sqrt{\left(\omega_p^2 + \omega_s^2\right)^2 - 4\omega_p^2\omega_s^2(1-k^2)}}{2(1-k^2)}} \quad (4)$$

If the circuit is designed such that primary and secondary side are matched to $\omega_p = \omega_s = \omega_0$, only two solutions exist for (4):

$$\omega_{1,2} = \frac{\omega_0}{\sqrt{1 \pm k}} \quad (5)$$

The power transfer efficiency yields a maximum between ω_1 and ω_2 and since the coupling coefficient $k \gg 0$, ω_1 and ω_2 are shifted away from ω_0. This phenomena is well known for coupled oscillators and is known as frequency splitting in the field of WPT.

In the following we will explain how this phenomena can be analyzed based on the more accurate numerical model of the coils.

3. Numerical Modelling

A 3D geometry (Figure 7) was built in COMSOL Multiphysics ® following the specifications given in [9]. The design goal was to maximize the mutual inductance, while avoiding its sensitivity to winding misalignment.

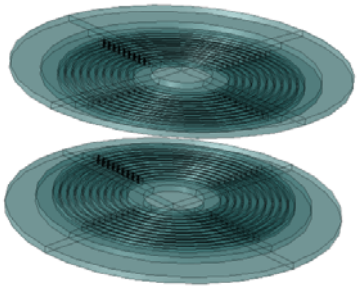

Figure 7. 3D model of a pair of disc coils, showing ferrite and aluminum discs next to the windings.

By using Ampere's Law, the magnetic vector potential A is calculated, and consequently the electrical potential V can be derived.

$$(j\omega\sigma - \omega^2\varepsilon_0)\vec{A} + \nabla \times \left(\frac{1}{\mu_0}\nabla \times \vec{A}\right) + (j\omega\varepsilon_0 + \sigma)\nabla V = \vec{J}_e \quad (6)$$

Spatial discretization of (6) via the finite element method (FEM) resulted in a model with 130.000 degrees of freedom (DOFs), i. e second order ordinary differential equations of the form:

$$\begin{aligned} M\ddot{x}(t) + E\dot{x}(t) + Kx(t) &= Fu(t) \\ y &= C_v\dot{x}(t) + C_P x(t) + Du(t) \end{aligned} \quad (7)$$

where $M, E, K \in \mathbb{R}^{n\times n}$, $F \in \mathbb{R}^{n\times m}$, $C_v, C_p \in \mathbb{R}^{p\times n}$, $D \in \mathbb{R}^{p\times m}$, $u \in \mathbb{R}^m$ is the input vector, $x \in \mathbb{R}^n$ is the state vector, and $y \in \mathbb{R}^p$ is the output vector.

The system matrices in (7) can be extracted by using Livelink™ for Matlab.

4. Model Order Reduction

The enormous computational effort for the solution of a full-scale model (7), prevents its co-simulation with an electrical circuitry and thus the efficient optimization of power transfer efficiency. Luckily, it turns out that model order reduction can yield a system of the same form as (7) but with only 20 DOFs, which is still highly accurate. It focuses on reducing the number of equations, while preserving the input-output behavior of the dynamical system. In the following, we explain how MOR works.

The model (7) can be rewritten as:

$$\begin{bmatrix} -K & 0 \\ 0 & M \end{bmatrix}\begin{pmatrix} \dot{z}(t) \\ \dot{z}(t) \end{pmatrix} = \begin{bmatrix} 0 & -K \\ -K & E \end{bmatrix}\begin{bmatrix} z(t) \\ \dot{z}(t) \end{bmatrix} + \begin{bmatrix} 0 \\ F \end{bmatrix}u(t)$$
$$y(t) = \begin{bmatrix} C_p & C_v \end{bmatrix}\begin{bmatrix} z(t) \\ \dot{z}(t) \end{bmatrix} + Du(t) \quad (8)$$

where the new matrices constitute a new transformed first-order system of the form:

$$\begin{aligned} E\dot{x}(t) &= Ax(t) + Bu(t) \\ y(t) &= Cx(t) + Du(t) \end{aligned} \quad (9)$$

By means of Laplace transform, the transfer function of (9) reads:

$$H(s) = C(A^{-1}Es - I)^{-1}A^{-1}B + D \qquad (10)$$

$H(s)$ can be developed into Taylor series and its coefficients are known as moments of the transfer function and are defined as:

$$M_i = C(A^{-1}E)^i A^{-1}B\ ,\ i = 0{,}1\ldots \qquad (11)$$

These moments are vectors or matrices, which belong to the Krylov subspaces, defined as:

$$\begin{aligned}\mathcal{K}_r &= span\{A^{-1}B, .., (A^{-1}E)^{n-1}A^{-1}B\}\\ \mathcal{K}_l &= span\{A^{-T}C^T, .., (A^{-T}E^T)^{n-1}A^{-T}C^T\}\end{aligned} \qquad (12)$$

$\mathcal{K}_r$ is called the right/input-sided Krylov subspace and $\mathcal{K}_l$ the left/output-sided Krylov subspace of order n.

MOR aims on finding a reduced system, whose first k moments will match the first k moments of the original system. This can be achieved by forming one or both Krylov subspaces of order k.

4.1. Reduction by Projection

By using matrices $V, W \in \mathbb{R}^{n\times k}$, a reduced model of order $k \ll n$ can be obtained for the original dynamical system of order n, as schematically represented in Figure 8.

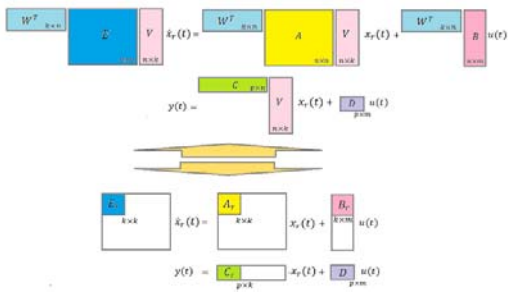

Figure 8. Order reduction of the first-order ordinary differential equation system (9).

If the columns of matrix V form the basis of the input-sided Krylov subspace and the columns of matrix W the basis of the output-sided Krylov subspace, the method is known as two-sided Krylov method.

On the other hand side, one can use only one basis (of $\mathcal{K}_r$ or of $\mathcal{K}_l$) and set $V = W$ for the projection. Then the method is known as the input-one-sided or the output-one-sided Krylov method.

4.2 Arnoldi Process

The Arnoldi process is one of the most popular algorithms to find an orthonormal basis for the input or output Krylov subspace and compute the matrices V or W respectively.

It is based on modified Gram-Schmidt orthogonalization as follows. Consider for example the Krylov subspace $\mathcal{K}_r$ of order k. The Arnoldi algorithm finds a set of vectors $v_1, v_2, \ldots, v_k$ with length one, which are orthogonal to each other and form the basis for the given Krylov subspace:

$$\begin{aligned}V^T V &= I\\ span\{v_1, v_2, \ldots, v_k\} &= \mathcal{K}_r\end{aligned} \qquad (16)$$

It is an iterative procedure, as in each step one more vector, orthogonal to all other previous vectors, is constructed and normalized.

The algorithm further generates an upper Hessenberg matrix $H_k \in R^{k\times k}$, which is related to the original system matrix A as:

$$V^T \cdot A \cdot V = H_k \qquad (17)$$

and can be interpreted as the matrix of the reduced system (e. g. the A_r in Figure 8). It can be easily proven [10] that such reduced system will match the first k moments of the original system (9).

4.3 Two-sided Arnoldi Algorithm

If the matrices V and W are computed as in (16) to be the orthonormal bases for the input, respectively output Krylov subspaces and are both used for the projection of the original system (as schematically represented in Figure 8), the method is called two-sided Arnoldi [11].

It yields better accuracy than the one-sided Arnoldi process, due to the fact that it matches $2k$ moments. Simultaneously the algorithm is

simpler and more stable than the alternative two-sided Krylov methods [12].

4.4 Block Arnoldi Algorithm

Block Arnoldi method is the extension of Arnoldi process for Multiple-Input-Multiple-Output (MIMO) systems. The algorithm implements the so called deflation, which is removing of linearly dependent vectors from V.

The deflation is controlled by checking whether the norm of each newly constructed vector is different from zero, after its orthogonalization.

4.5 Block Second Order Arnoldi Algorithm (SOAR)

The block SOAR method is basically an extension of the block Arnoldi method to second order systems. It employs the second order Krylov subspaces (corresponding to system (7)), defined in [12]:

$$\mathcal{K}_r(-K^{-1}E, -K^{-1}M, -K^{-1}F) \\ \mathcal{K}_l(-K^{-T}E^T, -K^{-T}M^T, -K^{-T}C^T) \tag{18}$$

where $\mathcal{K}_r$ is the right/input-sided and $\mathcal{K}_l$ is the left/output-sided second order Krylov subspace of order n.

If the columns of V form a basis for the input second order Krylov subspace, then the first k moments of the original and reduced models match [12], provided the reduced model is gained from (7) by projection analog to those schematically represented in Figure 8 and by setting e. g. $W = V$. The method is called one-sided block SOAR method.

If the columns of V and W form bases for the second order input and output Krylov subspaces, respectively, $2k$ moments of the original and reduced order systems match [12], provided the reduced model is gained from (7) by projection analog to those schematically represented in Figure 8. The reduction procedure is called two-sided block SOAR method.

The following results presented in section 5 are gained by using the one-sided and two-sided block SOAR methods respectively.

5. Simulation Results

Simulation experiments were conducted to evaluate the reference model in [9]. The reduced models stemming from the different SOAR methods (one-sided and two-sided) were compared to the full model. Finally a system-level simulation was performed with the purpose of characterizing a complete WPT system.

5.1 Sensitivity Analysis: 3D and 2D Comsol Models versus Reference Model

A model that was implemented in Ansys ® Maxwell [10], was selected as a reference. It was used to validate the results of the 3D model (from Figure 7), as well as two additional 2D axis-symmetric COMSOL models.

The first 2D model implements disc coils, considered as a bundle of stranded wires and modelled as multi-turn coils (see Figure 9).

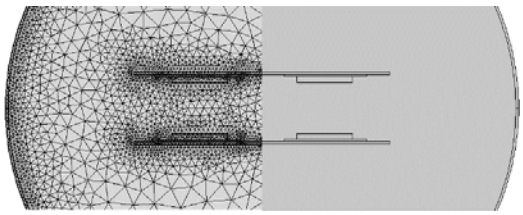

Figure 9. 2D axis-symmetric pair of disc coils. Left: spatial discretization, right: geometry

The second 2D model implements windings turns represented as concentric rings (see Figure 10).

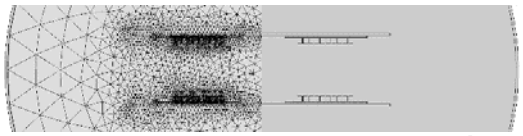

Figure 10. 2D axis-symmetric concentric windings. Left: spatial discretization, right: geometry

In each model, the vertical distance between coils was varied between 25 mm and 250 mm. This analysis was automated from Matlab™ by using a script. The operational frequency was set to 150 kHz.

As observed in Figure 11, the relative error for self-inductance does not exceed the threshold of 1.25 % for all models with regard to the reference model.

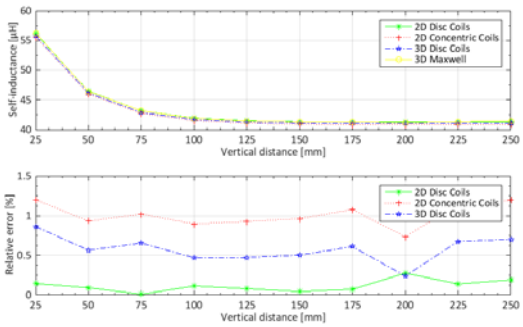

Figure 11. Self-inductance and relative error for different models, as vertical distance between coils was changed in the range of 25-250 mm.

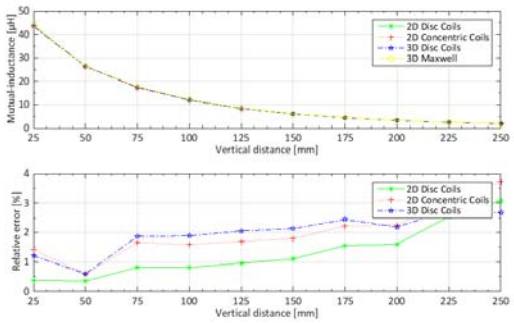

Figure 12. Mutual-inductance and relative error as vertical distance between coils was changed in the range of 25-250 mm.

The impact of misalignment on the mutual inductance was also evaluated. The error between models was lower than 4 %, as shown in figure 12.

5.2 Sensitivity Analysis of Reduced Models with Different Orders

The analysis was focused on comparing the accuracy of the implemented block SOAR algorithms versus the original full model. Reliability and accuracy of the algorithms were of outmost importance, as the reduced models were created with only a small number of moments (DOFs).

5.2.1. Input-sided Block SOAR Reduced Models

From the analysis of the coil's resistance in Figure 13, it can be observed that all reduced models with more than 4 moments are accurate. The maximal relative error was lower than 2.5 % for the reduced model with 7 moments.
Note, that the relative error for each reduced model is minimal in the vicinity of 1kHz, which was chosen the expansion point for the Taylor series of transfer functions.

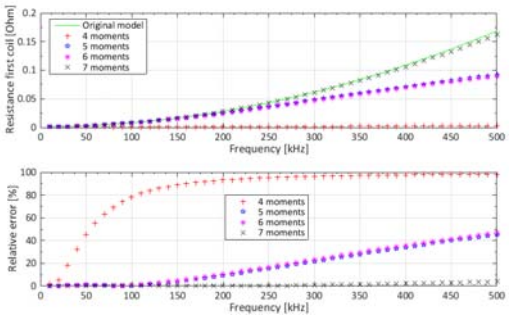

Figure 13. Sensitivity analysis for input-sided block SOAR reduced models with different number of moments; coil resistance (above) and relative error (bellow).

5.2.2. Output-sided Block SOAR Reduced Models

Models that are created by using output-sided SOAR show better accuracy than those constituted by input-sided SOAR algorithm, as shown in Figure 14. The model with 4 moments has the maximum relative error of 25 %. The model using 7 moments exhibits negligible error over the whole frequency range.

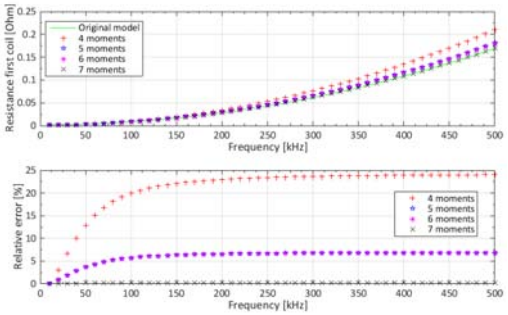

Figure 14. Sensitivity analysis for output-sided block SOAR reduced models with different number of moments; coil resistance (above) and relative error (bellow).

5.2.3. Two-Sided Block SOAR Reduced Models

As expected, models reduced by two-sided block SOAR are more accurate than those reduced by one-sided methods. The maximum relative error of reduction amounts to solely $5 \cdot 10^{-3}$% (see Figure 15).

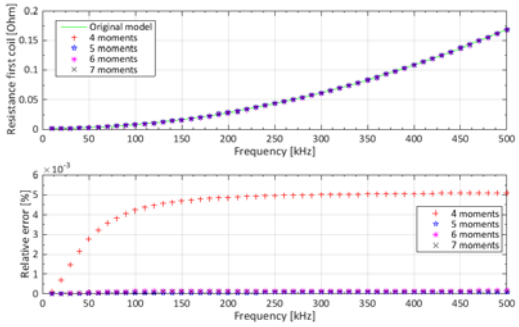

Figure 15. Sensitivity analysis for two-sided block SOAR reduced models with different number of moments; coil resistance (above) and relative error (bellow).

5.3 Power Efficiency Analysis

As a final step, power efficiency analysis was conducted on the reduced order models. For this purpose, the reduced models were exported to VHDL format and imported into ANSYS Simplorer® as 2-port networks (see Figure 16).

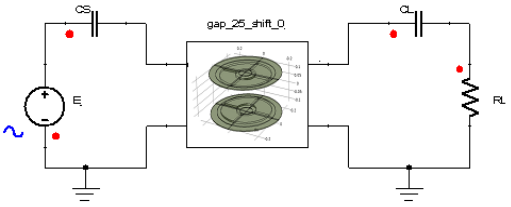

Figure 16. Reduced model connected as a 2-port network to an electrical circuit.

Apart from the voltage source E, each coil is connected to a serial capacitance CS and CL, and RL is the load resistance.

The voltage over the load resistor is shown in Figure 17, where frequency splitting around the operating frequency, 150 kHz is observed. The frequency splitting matches the analytically calculated values listed in Table 1.

Figure 18 depicts the power efficiency with its maximum within the frequency splitting range. As power efficiency is directly dependent on the coupling coefficient *k*, the bandwidth is affected when the vertical distance is increased.

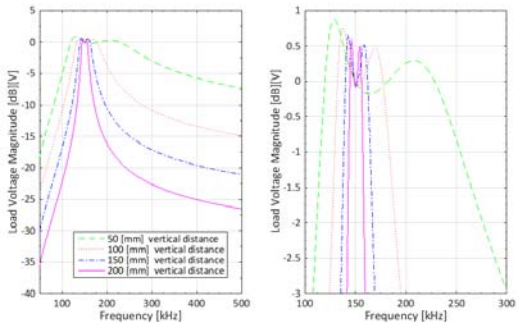

Figure 17. Load resistor voltage for several vertical distances (left); magnified view in the vicinity of the operating frequency of 150 kHz (right).

Table 1. Approximated calculated range of frequency splitting for horizontal displacements.

Horizontal displacement [mm]	$f_0/\sqrt{1+k}$ [kHz]	$f_0/\sqrt{1-k}$ [kHz]
0	132,34	177,36
50	134,50	172,49
100	140,02	162,46
150	146,44	153,83

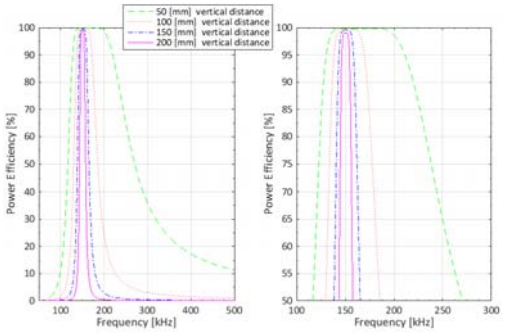

Figure 18. Power efficiency for several vertical distances (left); magnified view of the area with power efficiency larger than 50%

6. Conclusions and Outlook

Several models of the WPT coil setup were created in COMSOL ® based on the geometry suggested in [10]. The results for self- and mutual-inductance matched the reference model within 1.4 % and 4 %.

For creating reduced order models, the following block SOAR reduction algorithms (see chapter 4.5) were implemented and tested: input-sided, output-sided and two-sided. As expected, the two-sided algorithm yielded more accurate reduced order models than the one-sided algorithms.

Furthermore, reduced order models of very small size (between 4 and 7 second order ordinary differential equations) showed the same response as a full 3D model with more than 130 000 DOFs.

The effect of frequency splitting was analyzed analytically by calculating approximated values for the mutual inductance maxima. Those values were similar to the results obtained in ANSYS Simplorer®. Moreover, a continuous maximum in power transfer efficiency over the frequency splitting range was observed.

The next step would be to study the mathematical methods of parametric model order reduction [13] for their applicability to construct the reduced models in which the coil distance would be preserved as parameter [14], which would enable fast design optimization of WPT systems.

9. References

[1] Héctor Vázquez-Leal, Agustín Gallardo-Del-Angel, Roberto Castañeda-Sheissa and Francisco Javier González-Martínez (2012). The Phenomenon of Wireless Energy Transfer: Experiments and Philosophy, Wireless Power Transfer - Principles and Engineering Explorations, Dr. Ki Young Kim (Ed.), ISBN: 978-953-307-874-8, InTech, Available from: http://www.intechopen.com/books/wireless-power-transfer-principles-and-engineering-explorations/the-phenomenon-of-wireless-energy-transfer-experiments-and-philosophy.

[2] Morris Kesler. Highly Resonant Wireless Power Transfer: Safe, Efficient, and over Distance. White Paper [online].WiTricity Corporation, 2013. URL: http://www.witricity.com/assets/highly-resonant-power-transfer-kesler-witricity-2013.pdf

[3] Benedikt Schmuelling, Sarp G Cimen, Thomas Vosshagen, and Faical Turki, "Layout and Operation of a Non-Contact Charging System for Electric Vehicles," in 15th International Power Electronics and Motion Control Conference, EPE-PEMC 2012 ECCE Europe, Novi Sad, Serbia, 2012, p. 7.

[4] Aviva Brecher and David Arthur, "Review and Evaluation of Wireless Power Transfer (WPT) for Electric Transit Applications," Federal Transit Administration (FTA) Research, Washington DC, USA, FTA Report 60, 2014.

[5] André Kurs et al., "Wireless Power Transfer via Strongly Coupled Magnetic Resonances," *Science - AAAS*, vol. 317, pp. 83-86, July 2007.

[6] Xiaofang Yu et al., "Wireless power transfer in the presence of metallic plates: Experimental results," *AIP Advances*, 2013.

[7] Faical Turki and Abdelkader Guetif, "Contactless Charging Electric Vehicles with Renewable Energy," in *The fifth International Renewable Energy Congress IREC 2014*, Hammamet, Tunisia, 2014.

[8] Alexey Bodrov and Seung-Ki Sul, "Analysis of Wireless Power Transfer by Coupled Mode Theory (CMT) and Practical Considerations to Increase Power Transfer Efficiency," in *Wireless Power Transfer* -

Principles and Engineering Explorations. Rijeka, Croatia: InTech, 2012, ch. 2, p. 272.
[9] Z. Tang, M. Christini, T. Koga,“Wireless Power Transfer using Maxwell and Simplorer”, Automotive Simulation - World Congress, 2012.
[10] Roland W Freund, "Model reduction methods based on Krylov subspace," Acta Numerica, vol. 12, pp. 267-319, May 2003.
[11] B. Salimbahrami, B. Lohmann, T. Bechtold, J.G. Korvink, Two-sided Arnoldi algorithm and its application in order reduction of MEMS, in: I. Troch, F. Breitenecker (Eds.), Proc. 4th MATHMOD, Vienna, 2003, pp. 1021–1028.
[12] Behnam Salimbahrami, Rudy Eid, and Boris Lohmann, "Model Reduction by Second Order Krylov Subspaces. Extensions, Stability and Proportional Damping," in Conference on Computer Aided Control Systems Design, Munich, Germany, 2006, pp. 2997-3002.
[13] Panzer, Heiko; Mohring, Jan; Eid, Rudy; Lohmann, Boris, “Parametric Model Order Reduction by Matrix Interpolation”, at – Automatisierungstechnik 58 (8), 2010.
[14] Klis, D.; Burgard, S.; Farle, O.; Dyczij-Edlinger, R., “Fast Simulation of Wireless Power Transfer Systems With Varying Coil Alignment” *IFAC – PapersOnLine* 48 (1), 2015, pp. 248-253.